Effect of Spatial Wind Gradients on Airplane Aerodynamics

Dan D. Vicroy* and Roland L. Bowles*
NASA Langley Research Center, Hampton, Virginia

Wind shear is considered by many to be one of the major safety issues facing the aviation industry. The flight simulator is an important tool used to address the airborne aspects of wind-shear research. The fidelity of the analytical models that represent the airplane and the atmosphere within the flight simulatior environment is, therefore, of critical importance. This paper summarizes the results of recent studies investigating the effect of a spatially sheared wind field on airplane aerodynamics. The wind-shear effect was computed using a modified vortex-lattice computer program and characterized through the formulation of wind-shear aerodynamic coefficients. The magnitude of the aerodynamic effect was demonstrated by computing the resultant change in the aerodynamics of a conventional wing and stabilizer combination on a fixed flight path through a simulated microburst. In addition, a lateral dynamics analysis is presented that exemplifies the impact of derived wind-shear aerodynamic coefficients on aircraft stability. The results of this research indicate that a significant amount of the control authority of the airplane may be required to counteract the wind-shear-induced forces and moments in the microburst environment. The lateral dynamics analysis revealed new shear-dependent dynamic modes that may produce both aperiodic and oscillatory unstable motions.

Nomenclature

$\mathbf{A}$ = lateral stability derivative matrix
$a_{11}, a_{12}, \ldots$ = elements of $\mathbf{A}$ matrix
b = wing span, ft
$\mathbf{C}$ = shear coefficient slope $(\partial/\partial\alpha)$ matrix, per rad
C_D = drag coefficient, Drag/$q_\infty S$
C_L = lift coefficient, Lift/$q_\infty S$
C_l = rolling-moment coefficient, Rolling moment/$q_\infty Sb$
C_{l_ϕ} = roll stiffness coefficient $\partial C_l/\partial\phi$, per rad
C_{l_ψ} = yaw stiffness coefficient, $\partial C_l/\partial\psi$, per rad
C_m = pitching-moment coefficient, pitching moment/$q_\infty S\bar{c}$
C_n = yawing-moment coefficient, yawing moment/$q_\infty Sb$
C_Y = sideforce coefficient, sideforce/$q_\infty S$
$\bar{c}$ = mean aerodynamic chord, ft
$\mathbf{D}$ = shear coefficient intercept $(\alpha = 0)$ matrix
F_v = sidewash influence function, per ft
F_w = downwash influence function, per ft
I_{xx} = moment of inertia about the x body axis, slug − ft^2
I_{xz} = product of inertia, slug − ft^2
I_{zz} = moment of inertia about the z body axis, slug − ft^2
i = $\sqrt{-1}$
N = total number of vortex panels
p = roll rate about X-axis, rad/s
q_∞ = freestream dynamic pressure, lb/ft^2
r = yaw rate, rad/s
S = planform reference area, ft^2
s = wind shear, per s
U, V, W = velocity components in inertial axes system, ft/s
U_∞ = freestream velocity, ft/s
u_s, v_s, w_s = the body axes local wind velocity components due to wind shear, ft/s
u_w, v_w, w_w = relative wind velocity components in the body axes, ft/s
v = side velocity component in the body axes, ft/s
X, Y, Z = distance coordinates in the inertial axes system, ft
$\mathbf{X}$ = lateral state vector
$\dot{\mathbf{X}}$ = time rate of change of $\mathbf{X}$
x, y, z = distance coordinates in the body axes system, ft
α = angle of attack, rad
α_i = local angle of incidence, rad
β = sideslip angle, rad
Γ = vortex strength, ft^2/s
Δ = perturbation quantity
λ = taper ratio
ϕ = roll angle, rad
φ = planform dihedral angle, rad
ψ = yaw angle, rad

Subscripts

j = index for control point
n = index for elemental panel
o = value at $\alpha = 0$
s = value due to shear
ux = $\partial u_s/\partial x$ shear coefficient
uy = $\partial u_s/\partial y$ shear coefficient
uz = $\partial u_s/\partial z$ shear coefficient
vx = $\partial v_s/\partial x$ shear coefficient
vy = $\partial v_s/\partial y$ shear coefficient
vz = $\partial v_s/\partial z$ shear coefficient
wx = $\partial w_s/\partial x$ shear coefficient
wy = $\partial w_s/\partial y$ shear coefficient
wz = $\partial w_s/\partial z$ shear coefficient
α = change with angle of attack, $(\partial/\partial\alpha)$, per rad

Presented as Paper 88-0579 at the AIAA 26th Aerospace Sciences Meeting, Reno, NV, Jan. 11-14 1988; received April 11, 1988; revision received Sept. 12, 1988.

*Aerospace Technologist, Vehicle Operations Research Branch. Member AIAA.

Introduction

WIND shear is considered by many to be one of the major safety issues facing the aviation industry. There were 32

U.S. aircraft accidents or incidents, from 1964 through 1986, attributed to low-altitude wind shear. The crash of Delta flight 191 on August 2, 1985, which occurred while the plane was on an approach to landing at Dallas-Fort Worth International Airport and claimed 135 people, is the latest reminder of the danger of this weather phenomenon.

Wind shear is defined as any rapid change in wind velocity (speed or direction) over a relatively short distance at a particular time. Wind shear can be found in a variety of weather conditions such as gust fronts, sea-breeze fronts, and mountain waves, but is most often associated with the convective outflows of thunderstorms. One such convective activity is the microburst, which is a particularly lethal form of wind shear when encountered at low altitude. The microburst, which is discussed in detail in Ref. 1, is a strong localized downdraft of 2 to 5 m duration, which causes a significant outburst at or near the ground. The outburst usually extends less than 2.5 mi with peak winds as high as 168 mph.[1]

In January 1985, the Federal Aviation Administration began developing an integrated wind shear program plan[2] aimed at reducing the hazard of low-level wind shear. The program plan incorporates the expertise of industry, universities, and various government agencies such as NASA, the National Oceanic and Atmospheric Administration, and the Department of Defense into a 5-to-10 yr research and development effort. The objective of NASA's contribution to the wind shear program is to provide the technology base that will permit low-altitude wind-shear risk reduction through airborne detection, warning, and avoidance.

The flight simulator is an important tool used to address the airborne aspects of the wind-shear program. It is used for developing sensors, guidance, training, and operating procedures. The fidelity of the analytical models, which represent the airplane and the atmosphere within the flight simulator environment is, therefore, of critical importance.[3] NASA has developed high-fidelity models of three-dimensional, time-dependent, convective scale microbursts for simulator implementation. The bulk of the simulation and analytical studies conducted to date has used these and other wind-shear models to study the airplane performance effects. Very little work has been done to determine the effect of the three-dimensional spatial variation of the wind field about the airplane, on the airplane's aerodynamic characteristics. It is important that these aerodynamic effects are characterized and presented in a form that can be incorporated into research and training simulators.

This paper summarizes the results of recent studies investigating the effect of a three-dimensional, spatially sheared wind field on airplane aerodynamics. The wind-shear effect was computed using a modified vortex-lattice computer program and characterized through the formulation of wind-shear aerodynamic coefficients. The magnitude of the aerodynamic effect was demonstrated by computing the resultant change in the aerodynamics of a conventional wing and stabilizer combination on a fixed flight path through a simulated microburst. The results of a lateral dynamics analysis are presented that exemplify the impact of derived wind-shear aerodynamic coefficients on aircraft stability.

This paper is divided into four sections. The first is a brief description of the modifications required to the vortex-lattice program in order to incorporate the wind velocity gradients and compute their aerodynamic effect. This is followed by a section that defines the wind-shear aerodynamic coefficients. The next section presents the results of computed aerodynamic and lateral dynamic analysis. The final section summarizes the results and list recommendations for further research.

Modification of Vortex-Lattice Algorithm

A modified version of the vortex-lattice computer program presented in Ref. 4 was used to compute the wind-shear aerodynamic effect. The computer program presented in the reference was developed to compute the aerodynamic load distribution for single or dual planforms in a uniform flowfield. This program was modified to compute the load distributions resulting from nonuniform sheared flowfields. A brief description of the required modifications is discussed in the following sections.

Defining a Spatially Varying Wind Field

The local wind velocity for a uniform flowfield at a point defined in the body axis system, as shown in Fig. 1, can be written as

$$\begin{bmatrix} u_w \\ v_w \\ w_w \end{bmatrix} = -U_\infty \begin{bmatrix} \cos\alpha \cos\beta \\ \sin\beta \\ \sin\alpha \cos\beta \end{bmatrix} \tag{1}$$

The nonuniform flowfield was defined by adding the local wind velocities from the wind shear to the uniform flowfield equation.

$$\begin{bmatrix} u_w \\ v_w \\ w_w \end{bmatrix} = \begin{bmatrix} u_s \\ v_s \\ w_s \end{bmatrix} - U_\infty \begin{bmatrix} \cos\alpha \cos\beta \\ \sin\beta \\ \sin\alpha \cos\beta \end{bmatrix} \tag{2}$$

The local wind-shear velocity components (u_s, v_s, w_s) are defined in terms of the spatial wind velocity gradients as

$$\begin{bmatrix} u_s \\ v_s \\ w_s \end{bmatrix} \equiv \begin{bmatrix} \partial u_s/\partial x & \partial u_s/\partial y & \partial u_s/\partial z \\ \partial v_s/\partial x & \partial v_s/\partial y & \partial v_s/\partial z \\ \partial w_s/\partial x & \partial w_s/\partial y & \partial w_s/\partial z \end{bmatrix} \begin{bmatrix} x \\ y \\ z \end{bmatrix} \tag{3}$$

The effect of sideslip was not addressed within the limits of this study.

Boundary Condition

One of the fundamental conditions of the vortex-lattice program is the "no flow" condition at the control point of each vortex panel. This boundary condition simply states that no flow can pass through the vortex panel at the control point, thus requiring the flow to be tangent to the mean camber line of the surface. The control points are located at the three-quarter-chord, midspan point of each vortex panel. This boundary condition equation defines the vortex strength of each panel.

Details of the boundary condition modification required to incorporate the local shear velocity components are provided

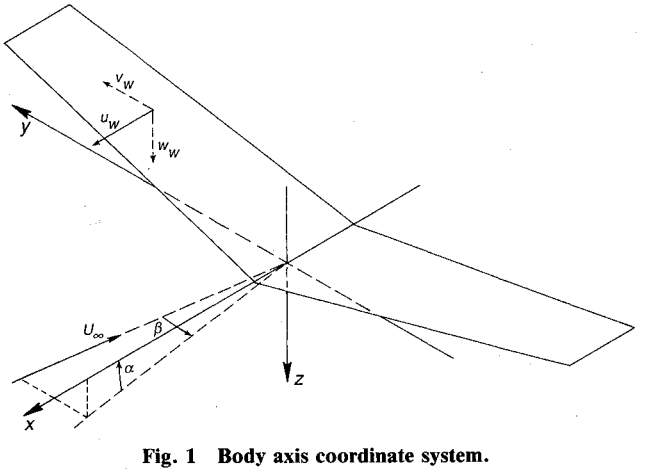

Fig. 1 Body axis coordinate system.

in Ref. 5. The modified boundary condition equation is

$$(F_w - F_v \tan\varphi)\frac{\Gamma}{U_\infty} = 4\pi\left[\alpha + \left(1 - \frac{u_s}{U_\infty}\right)\alpha_i + \frac{v_s}{U_\infty}\tan\varphi - \frac{w_s}{U_\infty}\right] \tag{4}$$

The influence functions (F_w, F_v) are only dependent upon the planform geometry and freestream Mach number and, therefore, required no modification for a nonuniform wind field. The development of the influence functions is provided in Ref. 4.

Note that the wind-shear velocities effectively act as an incremental change in the local angle of attack of the vortex panel. This is more clearly seen by rewriting the boundary condition as

$$(F_w - F_v \tan\varphi)\frac{\Gamma}{U_\infty} = 4\pi(\alpha + \alpha_i + \alpha_s) \tag{5}$$

where α_s is the incremental change in the local angle of attack due to the wind-shear velocities.

$$\alpha_s = -\frac{u_s}{U_\infty}\alpha_i + \frac{v_s}{U_\infty}\tan\varphi - \frac{w_s}{U_\infty} \tag{6}$$

The effect of the wind-shear distribution across the planform is, therefore, analogous to distorting the planform shape through twist or camber, as was noted in Ref. 6.

One of the basic limitations of vortex-lattice theory is that the results are restricted to small angles of attack where the viscous flow effects are assumed to be minimal. Because of this restriction, α_s must also be limited to small values. If the shear velocities are assumed to be of equal order of magnitude, then they must also be small relative to the freestream (u_s/U_∞, v_s/U_∞, $w_s/U_\infty \ll 1$) for any value of φ.

Since both α_i and u_s/U_∞ are small values, their product can be neglected from the boundary condition equation. For a vortex lattice of N elements, the boundary condition for a particular control point (j) can now be written as:

$$\sum_{n=1}^{N}(F_{w,n,j} - F_{v,n,j}\tan\varphi_j)\frac{\Gamma_n}{U_\infty} = 4\pi\left(\alpha + \alpha_{i,j} + \frac{v_{s,j}}{U_\infty}\tan\varphi_j - \frac{w_{s,j}}{U_\infty}\right) \tag{7}$$

The load distribution of the planform can be determined after solving this equation for the circulation of each horseshoe vortex.

Force and Moment Equations

The lift generated by a vortex element in uniform flow is determined by the components of the freestream, sidewash and downwash velocities perpendicular to the element. For nonuniform flow conditions, the shear induced velocity components (u_s, v_s, w_s) need to be incorporated into the lift equation. The details of this modification are provided in Ref. 5.

Shear Coefficient Development

In Ref. 7, Campos introduces a method of characterizing the aerodynamic effect of the individual shear components through the development of shear coefficients. The shear coefficients are the partial derivatives of the force and moment coefficients with respect to the individual velocity gradient and are nondimensionalized by a characteristic length and the freestream velocity. For example, the effect of shear on lift can be expressed in the form of a shear coefficient (C_{L_s}) defined as

$$C_{L_s} = \frac{\partial C_L}{\partial[s\bar{c}/(2U_\infty)]} \tag{8}$$

where the shear s is any one of the elements of the velocity gradient matrix of Eq. (3). This shear coefficient represents the distributed additional lift due to a velocity gradient about the planform. The total planform lift coefficient now has an additional term.

$$C_L = C_{L_\alpha}\alpha + C_{L_o} + \Phi_{\Sigma_\lambda}\frac{s\bar{c}}{2U_\infty} \tag{9}$$

However, the wind shear is not generally in the form of a single velocity gradient but rather a matrix of velocity gradients, as in Eq. (3). Consequently, the total lift coefficient will not have just one, but a series of additional terms due to the shear.

It can be shown, under the limiting assumptions and conditions in which the force and moment equations were derived, that the aerodynamic shear coefficients are linear functions of angle of attack and can be expressed in the form

$$C_{L_s} = C_{L_{\alpha_s}}\alpha + C_{L_{o_s}} \tag{10}$$

The development of this functional form is provided in Ref. 5.

Expressing the change in each of the aerodynamic coefficients (C_L, C_D, C_Y, C_l, C_m, and C_n) due to each of the velocity gradient terms yields the matrix equation

$$\begin{bmatrix} \Delta C_L(2U_\infty/\bar{c}) \\ \Delta C_D(2U_\infty/\bar{c}) \\ \Delta C_Y(2U_\infty/b) \\ \Delta C_l(2U_\infty/b) \\ \Delta C_m(2U_\infty/\bar{c}) \\ \Delta C_n(2U_\infty/b) \end{bmatrix} = [\alpha\mathbf{C} + \mathbf{D}] \begin{bmatrix} \partial u_s/\partial x \\ \Delta\partial u_s/\partial y \\ \partial u_s/\partial z \\ \partial v_s/\partial x \\ \partial v_s/\partial y \\ \partial v_s/\partial z \\ \partial w_s/\partial x \\ \partial w_s/\partial y \\ \partial w_s/\partial z \end{bmatrix} \tag{11}$$

where

$$\mathbf{C} = \begin{bmatrix} C_{L_{\alpha_{ux}}} & C_{L_{\alpha_{uy}}} & C_{L_{\alpha_{uz}}} & C_{L_{\alpha_{vx}}} & \cdots & C_{L_{o_{wx}}} \\ C_{D_{\alpha_{ux}}} & C_{D_{\alpha_{uy}}} & C_{D_{\alpha_{uz}}} & \cdot & \cdots & \cdot \\ C_{Y_{\alpha_{ux}}} & C_{Y_{\alpha_{uy}}} & \cdot & \cdot & \cdots & \cdot \\ C_{l_{\alpha_{ux}}} & \cdot & \cdot & \cdot & \cdots & \cdot \\ C_{m_{\alpha_{ux}}} & \cdot & \cdot & \cdot & \cdots & \cdot \\ C_{n_{\alpha_{ux}}} & \cdot & \cdot & \cdot & \cdots & C_{L_{o_{wz}}} \end{bmatrix} \tag{12}$$

$$\mathbf{D} = \begin{bmatrix} C_{L_{o_{ux}}} & C_{L_{o_{uy}}} & C_{L_{o_{vx}}} & C_{L_{o_{vx}}} & \cdots & C_{n_{\alpha_{wz}}} \\ C_{D_{o_{ux}}} & C_{D_{o_{uy}}} & C_{D_{o_{uz}}} & \cdot & \cdots & \cdot \\ C_{Y_{o_{ux}}} & C_{Y_{o_{uy}}} & \cdot & \cdot & \cdots & \cdot \\ C_{l_{o_{ux}}} & \cdot & \cdot & \cdot & \cdots & \cdot \\ C_{m_{o_{ux}}} & \cdot & \cdot & \cdot & \cdots & \cdot \\ C_{n_{o_{ux}}} & \cdot & \cdot & \cdot & \cdots & C_{n_{o_{wz}}} \end{bmatrix} \tag{13}$$

The aerodynamic effect of a sheared flowfield can now be characterized through the shear coefficients of matrices **C** and **D**.

Wind-Shear Aerodynamic Effect

The magnitude of the wind-shear aerodynamic effect was demonstrated using the wing and horizontal stabilizer configuration of a conventional commercial twin-jet. Figure 2 shows the wing and stabilizer planforms and the vortex panel distribution. The origin of the shear for the wing-only configuration was coincident with the aerodynamic center of the wing. The origin for the wing/stabilizer configuration was located at the quarter-chord location of the mean aerodynamic chord of the wing, which approximated the center of gravity of the airplane.

The wind-shear moment coefficients for the wing only and the wing/stabilizer are presented in Fig. 3. In general, the shear coefficients can be separated into longitudinal and lateral terms. The pitching moment coefficients had zero values for all but the $\partial u_s/\partial x$, $\partial u_s/\partial z$, $\partial v_s/\partial y$, $\partial w_s/\partial x$, and $\partial w_s/\partial z$ wind gradient terms. The lateral coefficients (rolling and yawing moment) had nonzero values for the remaining wind gradients ($\partial u_s/\partial y$, $\partial v_s/\partial x$, $\partial v_s/\partial z$, and $\partial w_s/\partial y$) and zero values for those shears that effected the pitching moment coefficients. The contribution of the horizontal stabilizer to the wind-shear coefficients in nearly every case resulted in an increase in the shear coefficient magnitude. As one might expect, the pitching moment shear coefficients were effected by the addition of the stabilizer, much more than were the lateral coefficients. The horizontal and vertical displacement of the stabilizer lead to the large increase in the x and z shear coefficient magnitude. Correspondingly, the y shear coefficients were much less effected by the addition of the horizontal stabilizer.

The wind-shear force coefficients exhibited similar trends as the moment coefficients. The force coefficients were omitted from this report for space considerations, but are presented in Ref. 5.

The magnitude of the wind-shear aerodynamic effect was demonstrated by computing the change in the total moment coefficients for the airplane when subjected to the wind shears of a microburst encountered on an approach to landing. This was accomplished by using the wind-shear coefficients presented in Fig. 3 for the wing and horizontal stabilizer. Figure 4 shows the location of the microburst relative to the path of the airplane.

The microburst wind field was generated from the three-dimensional numerical cloud model presented in Ref. 8. The wind field used for this study was of an axisymmetric mature microburst. The airplane traversed the microburst along a 3-deg glide slope, at 140 knots ground speed, with zero yaw, pitch, and roll. The earth-referenced velocity and shear components had to be transformed into airplane body axis components in order to compute their aerodynamic effect. The Euler angles (yaw, pitch, and roll) had to be specified for the axes transformation. As the airplane penetrated the microburst, the body referenced shear values varied from a minimum of -0.12 to a maximum of 0.15 s^{-1}. The true airspeed varied from 130 to 148 knots, and the change in angle of attack along the flight path was from -3 to 13 deg. The resultant change in the rolling, pitching, and yawing moment coefficients are shown in Fig. 5.

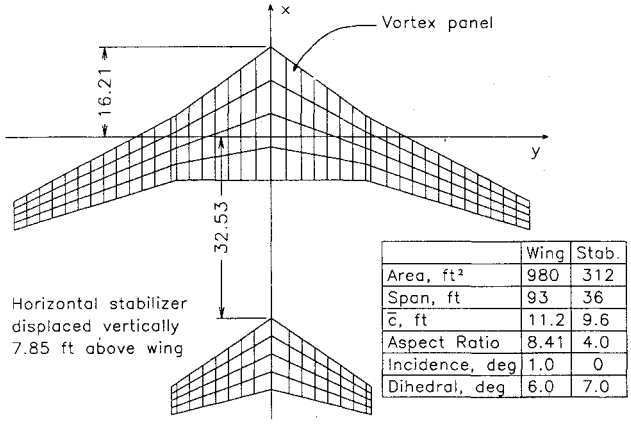

	Wing	Stab.
Area, ft²	980	312
Span, ft	93	36
$\bar{c}$, ft	11.2	9.6
Aspect Ratio	8.41	4.0
Incidence, deg	1.0	0
Dihedral, deg	6.0	7.0

Fig. 2 Vortex panel distribution on wing and stabilizer.

The pitching moment coefficient was the most effected by the wind-shear encounter, and the yawing moment was the least affected. All of the coefficients exhibited a similar response to the microburst wind field. As the airplane traversed the microburst vortex ring, a large rapid change in the coefficients resulted. Through the downburst portion the changes were more gradual and generally of a lesser magnitude; this was followed by another large rapid change as the airplane traversed the other end of the vortex ring.

In an effort to determine the significance of the wind-shear aerodynamic effect, the roll and pitch control authority of the twin-jet transport was compared with the rolling and pitching moments presented in Fig. 5. The results of this comparison, shown in Fig. 6, indicated that as much as 9% of the total roll control authority of the airplane (i.e., full aileron, spoilers, and rudder) would be required to counteract the wind-shear-induced rolling moment. Figure 7 shows the percent of elevator control required to counteract the wind-shear-induced pitching moment. It can be seen from this figure that as much as 21% of the control authority would be required to maintain the pitch attitude.

Wind-Shear Effect on Lateral Dynamics

The effects of wind shear on the airplane's dynamics can be determined by incorporating the wind-shear aerodynamic coefficients of Eqs. (11–13) into the small perturbation equations of motion. This has been done for the rolling motion equation, which, when fully expanded, produces a roll stiffness coefficient C_{l_ϕ} and a yaw stiffness coefficient C_{l_ψ}. These two coefficients depend explicitly on the earth referenced wind-shear gradients, having incorporated the transformation from the body-referenced to earth-referenced gradients into the coefficient equation. For a wing-only configuration in which the initial roll, bank, and yaw angles are zero, the coefficient equations are

$$C_{l_\phi} = \frac{b}{2U_\infty}\Bigg\{(C_{l_{\alpha_{uy}}}\alpha + C_{l_{o_{uy}}})\frac{\partial U}{\partial Z} + (C_{l_{\alpha_{vx}}}\alpha + C_{l_{o_{vx}}})\frac{\partial W}{\partial X} + [(C_{l_{\alpha_{vz}}} + C_{l_{\alpha_{wy}}})\alpha + (C_{l_{o_{vz}}} + C_{l_{o_{wy}}})]\left(\frac{\partial W}{\partial Z} - \frac{\partial V}{\partial Y}\right)\Bigg\} \tag{14}$$

$$C_{l_\psi} = \frac{b}{2U_\infty}\Bigg\{[(C_{l_{\alpha_{uy}}} + C_{l_{\alpha_{vx}}})\alpha + (C_{l_{o_{uy}}} + C_{l_{o_{vx}}})] \times \left(\frac{\partial V}{\partial Y} - \frac{\partial U}{\partial X}\right) - (C_{l_{\alpha_{vz}}}\alpha + C_{l_{o_{vz}}})\frac{\partial U}{\partial Z} - (C_{l_{\alpha_{vz}}}\alpha + C_{l_{o_{vz}}})\frac{\partial W}{\partial X}\Bigg\} \tag{15}$$

A rigorous analysis employing lifting line theory was conducted, which yielded results analogous to those given by Eqs. (14) and (15), namely

$$C_{l_\phi} = \frac{C_{L_\alpha}}{12}\left(\frac{1+3\lambda}{1+\lambda}\right)\frac{b}{2U_\infty}\left[\alpha\frac{\partial U}{\partial Z} + \left(\frac{\partial W}{\partial Z} - \frac{\partial V}{\partial Y}\right)\right] \tag{16}$$

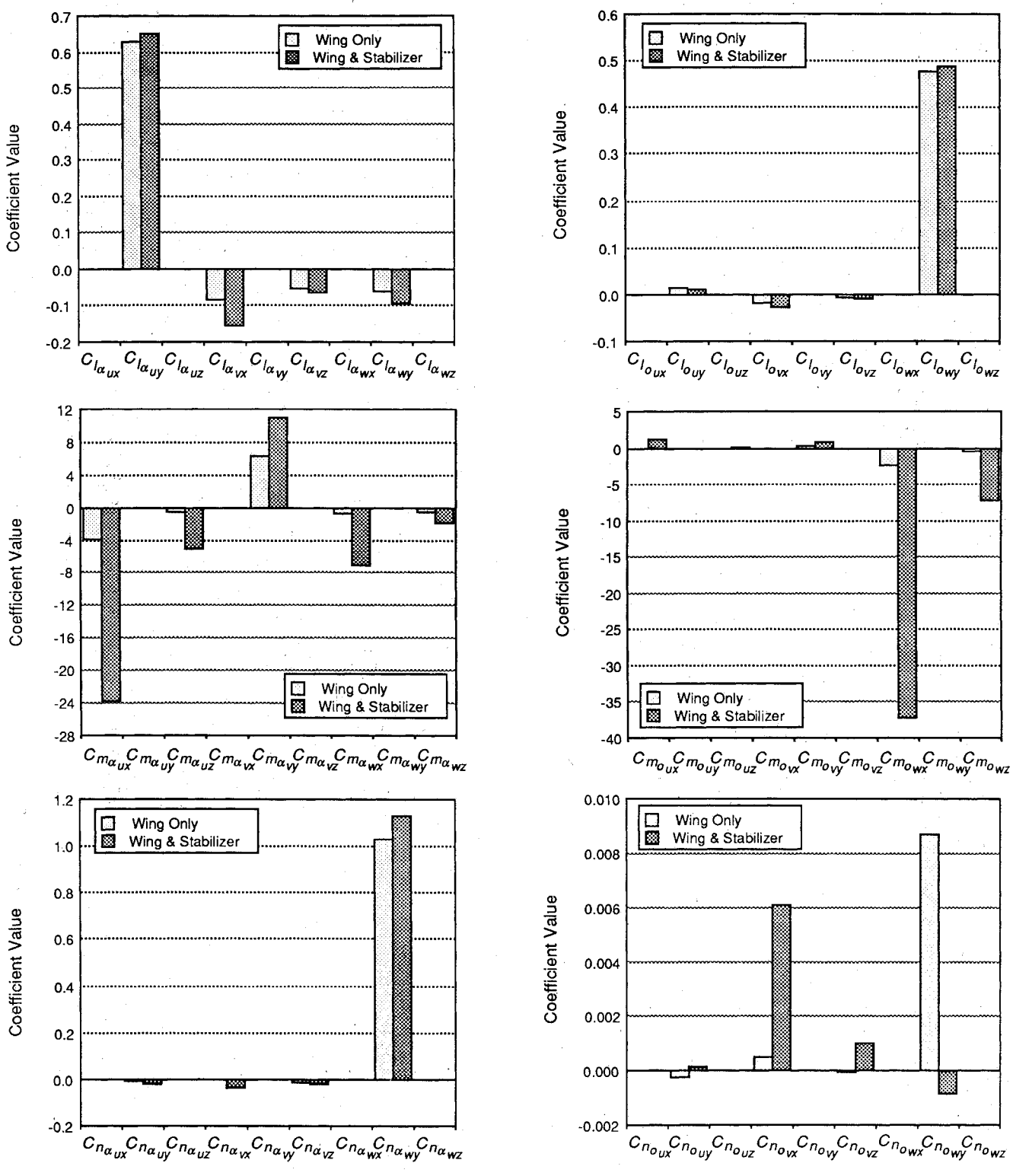

Fig. 3 Shear moment coefficients.

$$C_{l_\psi} = \frac{C_{L_\alpha}}{12}\left(\frac{1+3\lambda}{1+\lambda}\right)\frac{b}{2U_\infty}\left[\alpha\left(\alpha\frac{\partial V}{\partial Y} - \frac{\partial U}{\partial X}\right) - \frac{\partial W}{\partial X}\right] \tag{17}$$

where C_{L_α} is the lift curve slope, and λ is the wing taper ratio.

Examination of the magnitudes of the rolling moment shear coefficients presented in Fig. 3 show that all are small relative to $C_{l_{\alpha_{uy}}}$ and $C_{l_{o_{wy}}}$. Furthermore, a direct comparison of Eqs. (14) and (15) with Eqs. (16) and (17) reveals that $C_{l_{\alpha_{uy}}}$ and $C_{l_{o_{wy}}}$ are the only parameters predicted by lifting line theory. The numerical values for these two coefficients, derived from vortex-lattice and lifting line theory, are compared in Fig. 8. Quantitative agreement is considered good, given that the two computational methods involve fundamentally different assumptions.

If typical numbers are substituted into Eqs. (14–17), it can be seen that the magnitudes of C_{l_ϕ} and C_{l_ψ} are of the same order as C_{l_β} and C_{l_r}. Since C_{l_β} is an important derivative in determining aircraft handling quality characteristics, it is possible for sufficiently strong wind shear that the addition of the C_{l_ϕ} and C_{l_ψ} stability derivatives could create undesirable control situations for the pilot. These additional terms are

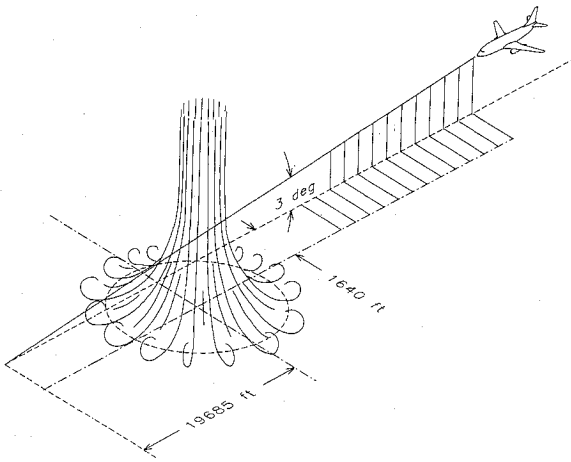

Fig. 4 Airplane flight path and microburst location.

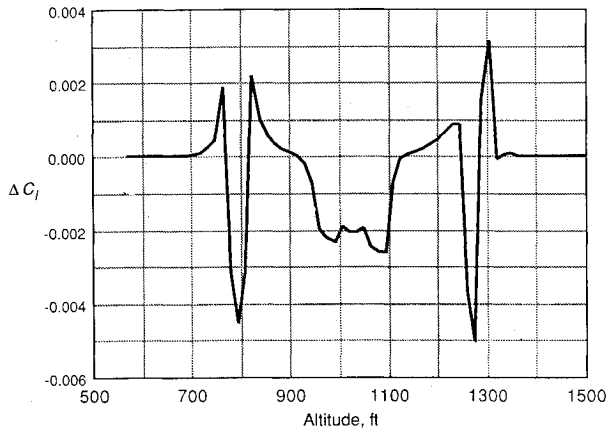

Fig. 5a Change in rolling moment coefficient due to microburst wind-shear components.

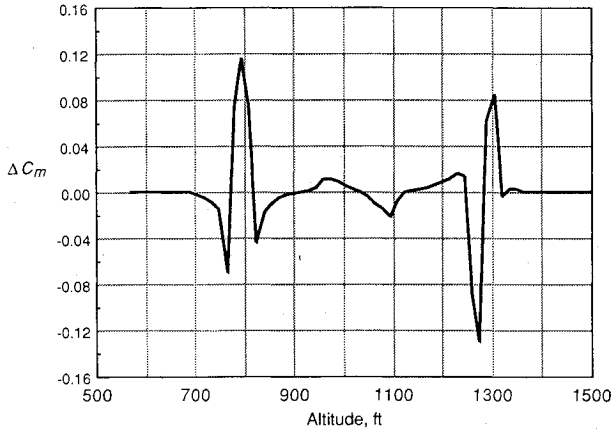

Fig. 5b Change in pitching moment coefficient.

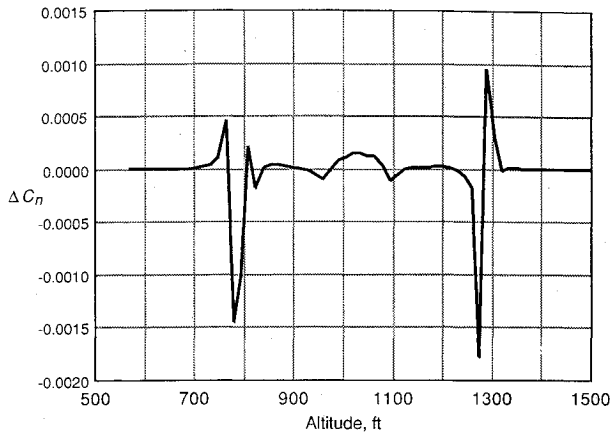

Fig. 5c Change in yawing moment coefficient.

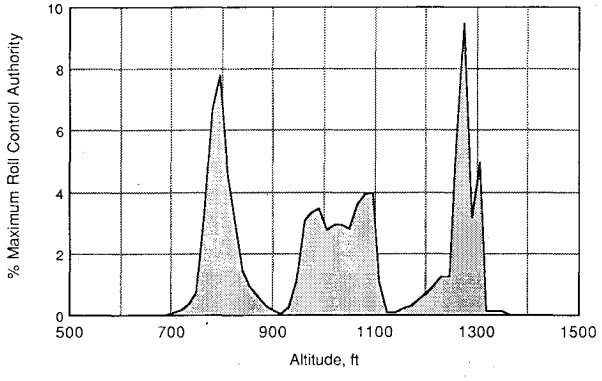

Fig. 6 Percent of total roll control authority required to counteract the wind-shear-induced rolling moment.

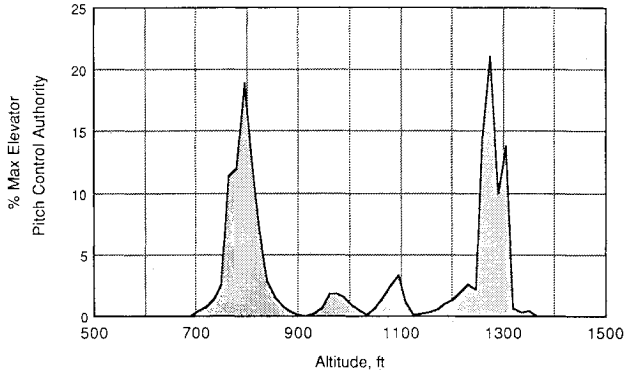

Fig. 7 Percent of elevator control authority required to counteract the wind-shear-induced pitching moment.

typically not modeled for aircraft motion analysis or included in flight simulator dynamics.

The lateral equations of motion for the twin-jet transport were modified to account for the effects of wind shear by including the stability derivatives C_{l_ϕ} and C_{l_ψ}. The modified lateral equations in state vector form are

$$\dot{\mathbf{X}} = \mathbf{AX}, \qquad \mathbf{X}^T = (v,p,r,\phi,\psi) \tag{18}$$

All of the **A** matrix elements except a_{24}, a_{25}, a_{34}, and a_{35} are conventionally defined stability derivatives. The others are wind-shear-induced stability derivatives of the form

$$a_{24} = q_\infty SbC_{l_\phi}\left(\frac{I_{zz}}{I_{xx}I_{zz}-I_{xz}^2}\right) \tag{19}$$

$$a_{25} = q_\infty SbC_{l_\psi}\left(\frac{I_{zz}}{I_{xx}I_{zz}-I_{xz}^2}\right) \tag{20}$$

$$a_{34} = q_\infty SbC_{l_\phi}\left(\frac{I_{xz}}{I_{xx}I_{zz}-I_{xz}^2}\right) \tag{21}$$

$$a_{35} = q_\infty SbC_{l_\psi}\left(\frac{I_{xz}}{I_{xx}I_{zz}-I_{xz}^2}\right) \tag{22}$$

Note that the **A** matrix reduces to conventional structure for uniform flow since $a_{24} = a_{25} = a_{34} = a_{35} = 0$.

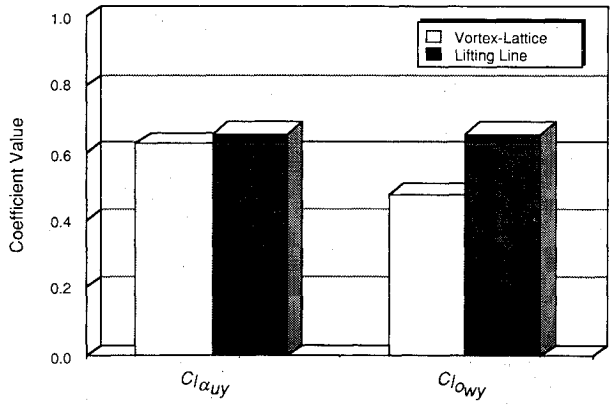

Fig. 8 Comparison of shear coefficient values computed by vortex-lattice and lifting line methods.

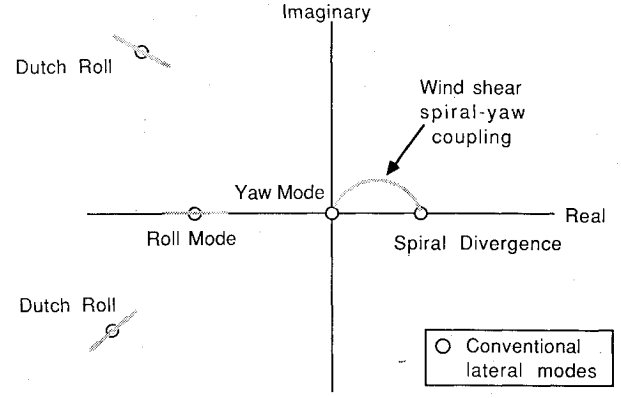

Fig. 9 Dynamic characteristics due to wind-shear-induced spiral-yaw coupling.

The eigenvalues of the stability matrix **A** were computed for the no-wind-shear condition, with the airplane trimmed in straight and level flight at an altitude of 1500 ft and 125 knots airspeed. The computed eigenvalues are

Dutch Roll Pair:	$-0.07964 \pm 1.139i$, s^{-1}
Roll Mode:	-2.017, s^{-1}
Spiral Divergence:	0.001681, s^{-1}
Directional:	0, s^{-1}

The impact of wind shear can be demonstrated by including C_{l_ϕ} and C_{l_ψ} in the eigenvalue calculation. For representative ranges of wind-shear gradients, the results indicate a 15 to 25% change in dutch roll damping and roll mode root placement. However, as seen in Fig. 9, a new dynamic characteristic is created as a direct result of spiral-yaw coupling. The newly created wind-shear mode produces both aperiodic and oscillatory motions, which can be stable or unstable depending on the magnitudes and sign of the wind-shear gradients. The eigenvalue distribution for the wind-shear-induced spiral-yaw mode is presented in Fig. 10. Examination of the figure suggests a wide variety of possible motions of significant complexity. Further work will examine the potential impact of these complex motions on transport flying qualities through expanded six-degree-of-freedom analyses and piloted simulation studies in wind-shear environments.

Concluding Remarks

Several pertinent results were established from the research presented in this paper.

1) A method of modifying a vortex-lattice algorithm to compute the wind shear aerodynamic effect was presented.

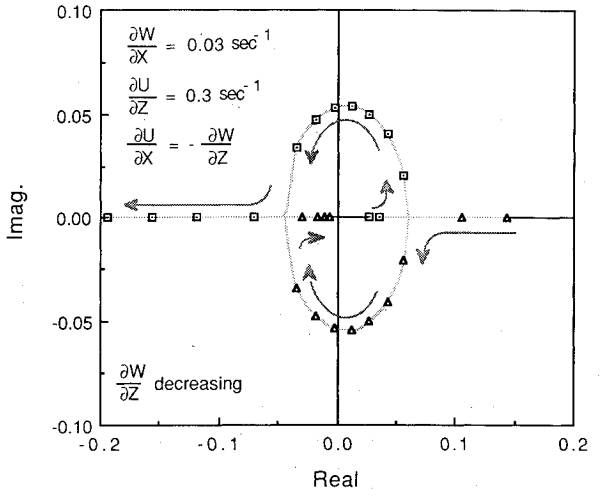

Fig. 10a Spiral-yaw mode eigenvalue distribution for $-0.3 \leq \partial W/\partial Z \leq 0.3\ s^{-1}$ in increments of $0.5\ s^{-1}$.

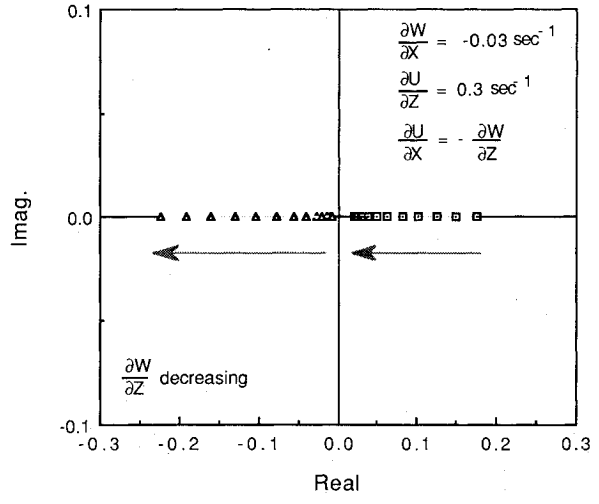

Fig. 10b Spiral-yaw mode eigenvalue distribution for $-0.3 \leq \partial W/\partial Z \leq 0.3\ s^{-1}$ in increments of $0.5\ s^{-1}$.

This approach should be directly applicable to more complex potential flow algorithms.

2) Wind-shear aerodynamic coefficients were formulated to characterize the wind-shear effect in a form that can be easily implemented into simulators.

3) An example of the magnitude of the wind-shear aerodynamic effect was demonstrated by computing the change in the aerodynamic coefficients of a conventional wing and stabilizer combination on a fixed flight path through a simulated microburst. The results indicate that a significant percent of available control authority may be required to counteract these effects.

4) Lateral dynamic analysis revealed new shear-dependent dynamic coefficients, the magnitude of which could produce large adverse changes in airplane handling qualities.

5) A spiral-yaw mode coupling may develop, producing both aperiodic and oscillatory unstable motions, depending on the magnitude and sign of the new dynamic coefficients and wind-shear gradients.

These results, however, are limited in several respects. The effect of sideslip angle was not accounted for in the formulation of the wind-shear aerodynamic coefficients. To account for this effect, an additional matrix of sideslip dependent wind-shear aerodynamic coefficients should be added to the formulation. The limits of potential flow theory restrict the results to the linear angle-of-attack range. The thin-wing approximation of vortex-lattice approach is an additional limita-

tion. Perhaps the greatest limitation of the study was the exclusion of the fuselage and vertical surface effects. The vertical surfaces (fin and rudder) should affect the lateral wind-shear aerodynamic coefficients in a similar manner as the horizontal stabilizer effected the longitudinal coefficients.

Several recommendations for future research can be derived from these results. Clearly, there is a need to adapt more sophisticated aerodynamic codes to compute the wind-shear effect of complete airplane configurations. The results presented earlier indicate that the wind-shear-induced forces and moments can impact the available control authority of the airplane. These effects need to be included in simulation studies to determine their impact on the pilot's ability to manage the flight path of the airplane during low-altitude wind-shear encounters. The impact of wind shear on the airplane's dynamic response need to be more fully understood, not only from a handling qualities perspective, but also in terms of the ramifications on control system design as well. Finally, there is a need for wind tunnel studies to confirm the analytical results and to explore the high-angle-of-attack effects.

References

[1]Fujita, T. T., "The Downburst," SMRP Research Paper 210, University of Chicago, Chicago, IL, 1985.

[2]"Integrated FAA Wind Shear Program Plan," DOT/FAA/DL, VS, AT-87/1, April 1987.

[3]Bowles, R. L. and Frost, W., "Wind Shear/Turbulence Inputs to Flight Simulation and Systems Certification," NASA CP-2474, July 1987.

[4]Margason, R. J. and Lamar, J. E., "Vortex-Lattice Fortran Program for Estimating Subsonic Aerodynamic Characteristics of Complex Planforms," NASA TN D-6142, 1971.

[5]Vicroy, D. D., "Influence of Wind Shear on the Aerodynamic Characteristics of Aircraft Using a Vortex-Lattice Method," NASA TP 2827, 1988.

[6]Vidal, R. J., "The Influence of Two-Dimensional Stream Shear on Airfoil Maximum Lift," *Journal of Aerospace Sciences,* Vol. 29, Aug. 1962, pp. 889–904.

[7]Campos, L. M. B. C., "On the Influence of Atmospheric Disturbances on Aircraft Aerodynamics," *Aeronautical Journal,* July 1984, pp. 257–264.

[8]Proctor, F. H., "The Terminal Area Simulation System, Volume I and Volume II," NASA CR 4046/4047, April 1987.